CHEMISTRY OF MATERIALS
Cite This: Chem. Mater. 2019, 31, 2635−2643
Article
pubs.acs.org/cm

Cu-Catalyzed Synthesis of CdZnSe−CdZnS Alloy Quantum Dots with Highly Tunable Emission

Yucheng Yuan,[†] Hua Zhu,[†] Xudong Wang,[‡] Dingzhou Cui,[†] Zehua Gao,[†] Dong Su,[§] Jing Zhao,[‡] and Ou Chen*[,†]

[†]Department of Chemistry, Brown University, 324 Brook Street, Providence, Rhode Island 02912, United States
[‡]Department of Chemistry, University of Connecticut, 55 North Eagleville Rd., Storrs, Connecticut 06269, United States
[§]Center for Functional Nanomaterials, Brookhaven National Laboratory, 735 Brookhaven Avenue, Upton, New York 11973, United States

Supporting Information

ABSTRACT: Fabrication of quantum dots (QDs) with emission covering a wide spectral region has been persistently intriguing because of their potentials in a range of practical applications such as biological labeling and imaging, solar cells, light-emitting diodes, and next-generation displays. In this work, we report the synthesis of CdZnSe−CdZnS core−shell alloy QDs through a Cu-catalyzed solid solution alloying strategy starting from CdSe−CdS core−shell QDs. The resulting CdZnSe−CdZnS alloy QDs exhibit emission profiles covering a wide wavelength range of 470−650 nm while maintaining high photoluminescence quantum yields. In addition, high morphological uniformity of the starting CdSe−CdS QDs can be largely retained in the final alloy QDs. We attribute this alloying process to the high mobility nature of Cu cations in Cd-chalcogenide crystals at elevated reaction temperatures, which allows Cu cations to act as transporting agents to transfer a Zn component into the CdSe−CdS QDs while maintaining the particle integrity. We show that this unique alloying strategy is independent of the shape of the starting QDs and can also be applied to the synthesis of CdZnSe−CdZnS nanorods. We anticipate that our study will instigate the synthesis of various high-quality alloy QDs and other alloy nanocrystals beyond what can be achieved currently.

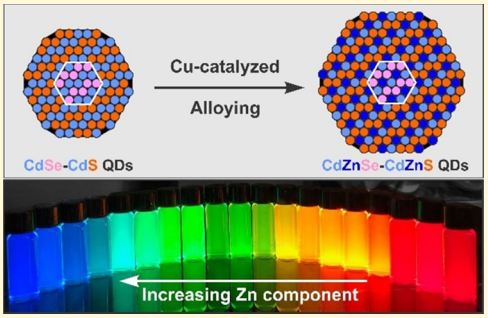

INTRODUCTION

Semiconductor quantum dots (QDs) exhibit unique properties including high absorbance cross section, broad excitation spectrum, tunable emission profile, high photoluminescence quantum yield (PL QY), and superior photochemical/physical stability.[1,2] These properties offer QDs great potential in diverse practical applications including solar energy harvesting,[3−8] biological imaging and labeling,[9−13] light-emitting diodes, and next-generation displays.[14−23] As a result, synthesizing QDs with uniform size, different shapes, high PL QY, and tunable and narrow emission spectrum have been a long-lasting active research topic and largely investigated in the past 3 decades.[24−49] One of the most profound discoveries toward improving the optical properties of QDs is through epitaxial deposition of shell semiconductor materials, especially with a wider band gap compared to that of the core QDs (also known as type-I core−shell QDs).[1,35,50] To date, various type-I core−shell QD systems have been synthesized and reported,[35] among which CdSe−ZnS, CdSe−CdS, and CdS−ZnS core−shell QDs are arguably the most studied ones with great synthetic control and superior optical performance.[39,51,52] However, because of the intrinsic properties of the core and shell materials, these core−shell systems either can only emit photons covering a limited range of the visible spectrum (i.e., CdSe−CdS and CdS−ZnS systems)[39,52,53] or possess a large lattice mismatch between the core and shell materials (i.e., CdSe−ZnS system), which usually limits the morphological uniformity and optical properties of the obtained core−shell QDs.[51,54] To this extent, alloying core and/or shell compositions of QDs has later been realized as an efficient means to enlarge spectral coverage as required in many of their potential applications.[55,56] In addition, by choosing appropriate alloy compositions, the band gap alignment and lattice mismatch between the core and shell materials can be widely tuned and optimized for desired optical properties.[57−67] To date, a variety of alloy QD systems have been reported through either simultaneous injection of the required precursors[55,58,61,62,64] or post-core-synthetic cation exchanges.[56,63,65] Especially, it is known that when CdZnSe alloy QDs serve as cores, a wide range of spectral tunabilities from deep blue to dark red can be achieved by altering the ratio of Cd and Zn compositions.[65,68] However, unlike CdSeS alloy QDs which are relatively easy to be fabricated because of minimal lattice mismatch (3.9%), the synthesis of CdZnSe QDs has proven to be challenging because of their relatively large crystal

Received: February 7, 2019
Revised: March 20, 2019
Published: March 21, 2019

DOI: 10.1021/acs.chemmater.9b00557
Chem. Mater. 2019, 31, 2635−2643

lattice mismatch (8.0%) between CdSe and ZnSe materials and unbalanced reactivities of commonly used Cd and Zn precursors.[55,56]

RESULTS AND DISCUSSION

In this work, we report a new synthetic paradigm for the fabrication of CdZnSe−CdZnS core−shell alloy QDs through a Cu-catalyzed solid solution alloying strategy. Taking advantage of the high mobility of Cu cations, we demonstrate that the Zn component can be transported into the starting CdSe−CdS core−shell QDs even using a relatively less reactive Zn precursor (i.e., Zn-oleate). We show that the obtained CdZnSe−CdZnS alloy QDs can emit at a wide range of wavelengths with the peak center covering a nearly full visible spectral region (470−650 nm) while maintaining high PL QYs (>50%). By monitoring the reaction process, we propose a new alloying mechanism highlighting the unique "catalytic" role Cu cations played in the process. In addition, we demonstrate that the surface defects caused by the remaining Cu cations in the CdZnSe−CdZnS alloy QDs can be effectively removed through a post-synthetic treatment with trioctylphosphine (TOP) based on hard and soft acids and bases (HSAB) theory. Finally, this approach can be easily adapted to the synthesis of the CdZnSe−CdZnS alloy nanorod (NR) system, suggesting its generality.

The starting CdSe−CdS core−shell QDs were synthesized following a previously reported method with minor modification (see the Supporting Information and Figure S1).[39] For the typical synthesis of alloy QDs (see synthetic details in the Supporting Information), 10 mg (~11.5 nmol) of CdSe−CdS core−shell QDs, 2.5 mL of 1-octadecene (ODE), and 2.5 mL of oleylamine (OAm) were treated with 0.1 mL of 0.5 mM $Cu(acac)_2$/OAm (~4 Cu per QD) at 240 °C for 20 min, followed by a slow injection of Zn-oleate (0.1 M in ODE) and 1-dodecanethiol (0.1 M in ODE) with a rate of 0.4 mL/h at 330 °C, simultaneously. The alloying process was monitored by absorption and PL spectroscopy measurements. During the process, the first absorption feature (PL peak) continuously blue-shifted from 600 to 493 nm (610−509 nm) (Figure 1a,b), indicating an increase of the band gap of QDs, which was attributed to the incorporation of Zn^{2+} cations into the CdSe−CdS core−shell QDs. The decrease (increase) of absorbance in the wavelength range of 400−500 nm (below 400 nm) indicated the incorporation of ZnS with a larger band gap (i.e., 3.91 eV) in the CdSe−CdS QDs. Although the PL QY of the QDs remained above 50% (Table S1), the full width at half-maximum (fwhm) of the PL peak increased from ~22 nm (~74 meV) to ~28 nm (~122 meV) and then decreased to ~23 nm (~113 meV) (Figure 1c). The initial increase of the PL fwhm was unlikely due to an inhomogeneous broadening effect as high morphological uniformity of the core−shell QDs was preserved during the entire alloying process evidenced by both transmission electron microscopy (TEM) and PL excitation (PLE) measurements (Figure 1a, inset, and Figure 2a−f).[39,69] Accordingly, we attribute this PL broadening effect to the homogeneous broadening caused by Cu-induced defects (e.g., crystal defects and unbalanced charges) inside the particles, as well as enhanced internal electrical field and enlarged dipole moment caused by a spontaneous polarization of the wurtzite (WZ) crystal structure while developing particle shape anisotropy (discussed below).[44,70−72]

To further confirm the alloying process and characterize the final QDs, X-ray diffraction (XRD) measurements were performed. The QDs unambiguously showed a WZ crystal structure with the fingerprint Bragg diffraction peaks of $(10\bar{1}2)$ and $(10\bar{1}3)$, demonstrating the epitaxial incorporation of ZnS (Figure 2g). However, all Bragg peaks red-shifted to higher angles during the growth, indicating a continuous shrinkage of the unit cell lattice (Table S2), consistent with the smaller WZ lattice parameters (a = 3.82 Å, c = 6.26 Å) of ZnS. In addition, the (0002) diffraction peak became narrower during the reaction (Figure 2h), indicating the preferential growth along the [0002] direction.[30−32,73] The ZnS growth was further confirmed by the increase of particle size from 7.7 ± 0.6 nm for the starting QDs to 11.9 ± 0.9 nm for the final particles determined by the TEM measurements (Figures 2a−f and S2). Instead of retaining the spherical shape, the particles became elongated with an aspect ratio of ~1.2 for the final obtained QDs (Figure 2f), in accordance with the favored [0002] growth direction. To verify the alloy core−shell structure of the QDs, high-angle annular dark-field scanning TEM (HAADF-STEM) was employed to map out the atomic distributions of Cd, S, Se, and Zn atoms. The energy-dispersive X-ray (EDX) spectroscopy elemental mapping result clearly showed that Cd and S atoms were distributed in the entire QDs, whereas Se atoms were located at the center of the particles throughout the alloying process, suggesting an intact anionic core−shell framework (Figures 2i and S3, Table S3).[74] Interestingly, unlike traditional core−shell growth, Zn atoms were also distributed in the entire particles and not only at the outer layer as a shell (Figure 2i).

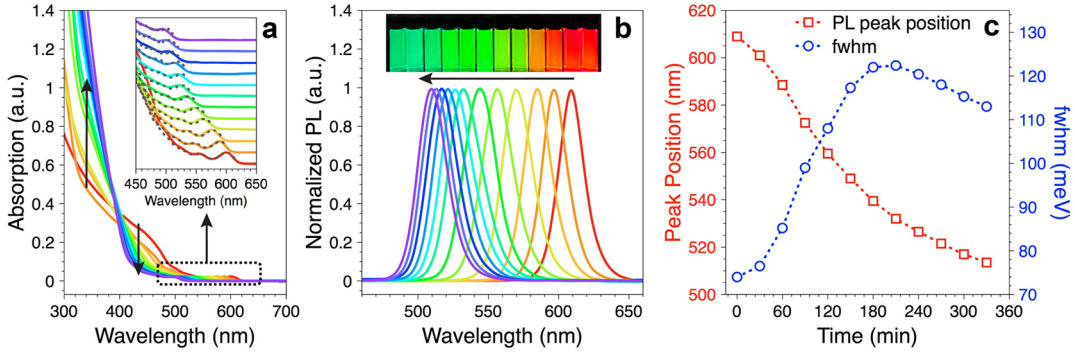

Figure 1. (a) Absorption spectral evolution during the synthesis of CdZnSe−CdZnS core−shell alloy QDs. Inset: zoomed-in spectra showing the blue shift of core absorption feature (solid line) and the corresponding PLE (dashed line). (b) PL spectral evolution during the synthesis. Inset: photograph of the aliquots taken during the synthesis under UV light illumination. (c) Peak position (red open square) and fwhm (blue open circle) of the PL profile as a function of reaction time.

DOI: 10.1021/acs.chemmater.9b00557
Chem. Mater. 2019, 31, 2635−2643

These results unambiguously led to the conclusion that a Zn alloying process instead of epitaxial shell growth took place during the reaction. This conclusion was in accordance with the continuous blue shift of both absorption and PL features as shown in Figure 1a,b.

Inductively coupled plasma atomic emission spectroscopy (ICP-AES) and EDX spectroscopy were employed to further determine the atomic percentages of Cd and Zn components for the core−shell QDs. As shown in Figure 3a, the atomic percentages of Cd and Zn measured by ICP-AES and EDX spectroscopy showed a high consistency. ICP data showed an increase of Zn percentage from 0 to ~74.3% and a corresponding decrease of Cd percentage from unity to ~25.7% as the reaction progressed (Figure 3a). To evaluate if the final particles were homogeneous or gradient alloys, the experimentally determined Cd and Zn atomic percentages were compared with the calculated values from the corresponding XRD patterns (Table S2) on the basis of Vegard's law.[75] The percentage offsets between the calculated and the experimentally determined values indicated that the core−shell QDs were not a homogeneous cationic solid solution but a partial gradient alloy of Zn component instead (Figure 3a). To quantify the partial alloying level, we express the cation alloying degree (A) of CdZnSe−CdZnS QDs as $A = (X_{Zn}/X_{Cd})/(Zn/Cd)_{nom}$, where X_{Zn} and X_{Cd} are the percentages of Zn and Cd atoms calculated based on the XRD data, and $(Zn/Cd)_{nom}$ is the atomic ratio of Zn and Cd obtained from ICP-AES measurements.[76] Note that the core and core−shell interface effects were ignored because of the relative small volume of the CdSe or CdZnSe cores (less than 5% of the total particle volume). On the basis of this calculation, the alloying degree of the CdZnSe−CdZnS QDs increased from 44.4% after 30 min of Zn and S precursor

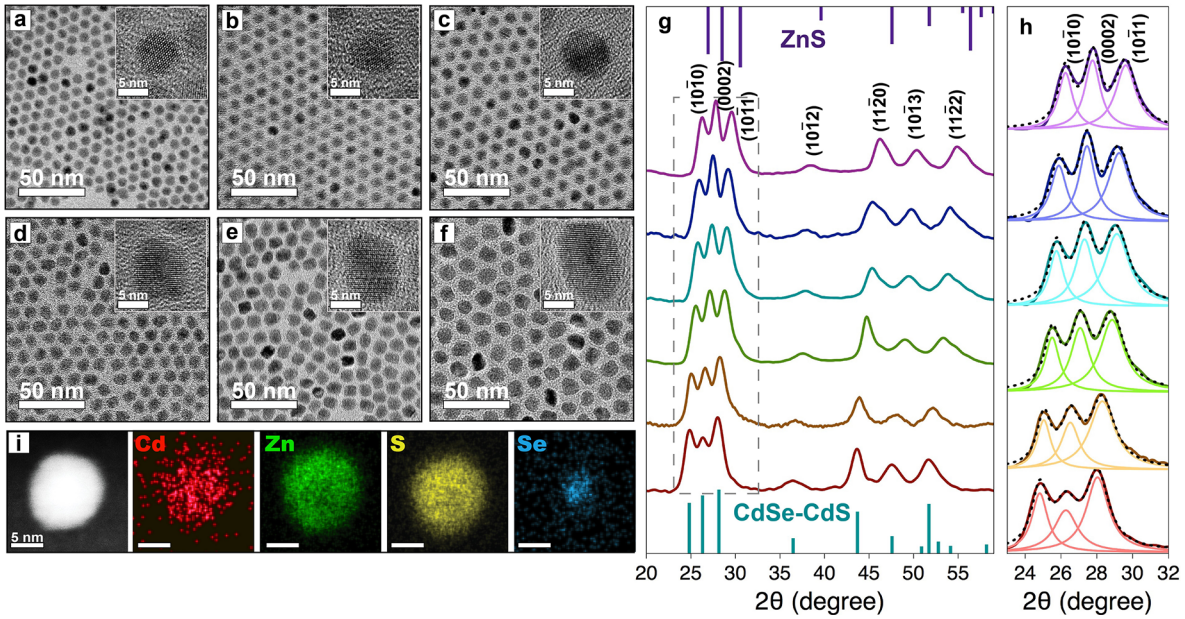

Figure 2. TEM images of starting CdSe−CdS core−shell QDs (a) and CdZnSe−CdZnS core−shell alloy QDs (b−f) with different amounts of Zn precursor addition [(b) 0.02 mmol, (c) 0.06 mmol, (d) 0.10 mmol, (e) 0.12 mmol, and (f) 0.22 mmol]. Insets are HR-TEM images of these QDs. (g) XRD spectral evolution during the synthesis of CdZnSe−CdZnS alloy QDs. The green and purple sticks show the positions of XRD peaks for the starting CdSe−CdS QDs and bulk WZ-ZnS, respectively. (h) Zoomed-in XRD spectra of the rectangular area in (g) to show (10$\bar{1}$0), (0002), and (10$\bar{1}$1) peaks with the fitted constituent peaks. (i) HAADF-STEM image and the corresponding EDX spectroscopy elemental mappings for one CdZnSe−CdZnS alloy QD.

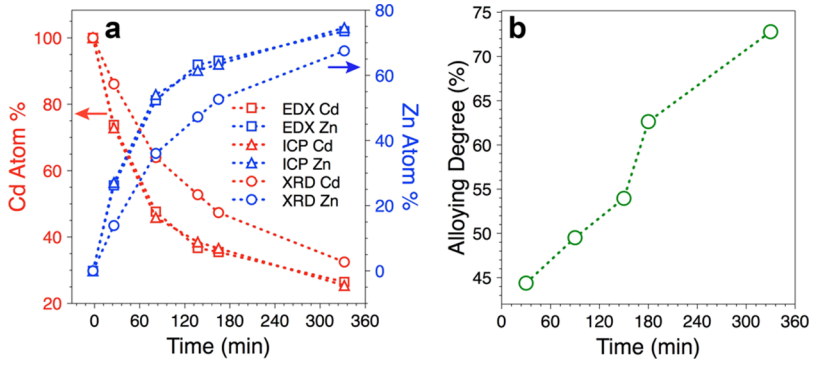

Figure 3. (a) Cd (red dotted lines) and Zn (blue dotted lines) atomic percentage evolutions based on EDX (open square), ICP (open triangle), and XRD (open circle) analyses. See detailed analysis data in the Supporting Information. (b) Zn-alloying degree evolution in the CdZnSe−CdZnS alloy QDs as a function of reaction time.

DOI: 10.1021/acs.chemmater.9b00557
Chem. Mater. 2019, 31, 2635−2643

injection to 72.8% of the final core−shell QDs. This increase of alloying degree can be ascribed to the high temperature (i.e., 330 °C) and longtime annealing effect during the course of the reaction (Figure 3b).[77]

It is very interesting that unlike conventional core−shell QD growth,[39,52] a concurrent alloying process occurred during the addition of Zn and S precursors in our reaction system. The obvious difference as compared to the reaction conditions for conventional core−shell growth was a Cu precursor treatment of the starting core−shell QDs (see the Supporting Information). Therefore, it is straightforward to hypothesize that Cu cations play the vital role in the observed alloying process. To confirm the necessity of Cu cations in the reaction, a control experiment without adding the Cu precursor was carried out while maintaining other reaction conditions for the growth of ZnS (see details in the Supporting Information). No obvious Zn-alloying effect was observed during the reaction as proved by both optical and TEM measurements (Figures S4 and S5). It was remarkable that only about 4 Cu per CdSe−CdS QD in average could make such a difference in achieving the CdZnSe−CdZnS core−shell alloy QDs, which stimulated us to further investigate the mechanism of this alloying process. First, the sample kept electron paramagnetic resonance (EPR) silent throughout the entire reaction (Figure S6), suggesting that Cu^{2+} was quickly reduced to Cu^{+} in the presence of electron-rich solvent and ligand (i.e., ODE and OAm) under the synthetic condition used in this study.[78−80] These Cu^{+} cations can occupy Cd sites substitutionally in the CdSe−CdS QDs rather to be in interstitial positions.[77] Second, the effective ionic radius of Cu^{+} (77 ppm) is nearly identical to that of Zn^{2+} (74 ppm) and is ~20% smaller than the radius of Cd^{2+} (95 ppm), suggesting a possible two-step process of Cd-to-Cu followed by Cu-to-Zn exchanges.[81] Last, the diffusion coefficient of Cu^{+} ions in a CdS single crystal can be calculated based on eq 1[77]

$$D = 2.1 \times 10^{-3}\, e^{-(0.96\ \mathrm{eV}/kT)}\ \mathrm{cm}^2/\mathrm{s} \quad (1)$$

where k is the Boltzmann constant, 8.617×10^{-5} eV/K, and T is the temperature. At a reaction temperature of 330 °C, the diffusion coefficient of Cu ions was calculated to be ~2000 nm^2/s. This calculated result suggested that Cu^{+} ions can diffuse across the entire QDs in only ~7 ms for the initial CdSe−CdS QDs (a diameter of 7.7 nm) and ~18 ms for the final CdZnSe−CdZnS alloy QDs (a diameter of 11.9 nm) under the reaction condition (see the Supporting Information). Meanwhile, the diffusion coefficient of Cu^{+} ions in CdS is about 4 orders of magnitude smaller at room temperature than at the reaction temperature (i.e., 330 °C), which implies the need of the high reaction temperature (see calculation details in the Supporting Information).[77] All the statements listed above lead us to hypothesize a possible Cu-catalyzed solid solution alloying mechanism for the formation of CdZnSe−CdZnS core−shell alloy QDs (Figure 4). In this process, initially, a small amount of Cu_2S can grow on the surface of CdSe−CdS QDs (Figure 4i), followed by the growth of a layer of ZnS (Figure 4ii). Subsequently, Cu ions can diffuse into the particles through Cd-to-Cu cation exchanges (Figure 4ii), followed by the occurrence of Cu-to-Zn cation exchange (Figure 4iii). In this two-step cation exchange process, the Cu ions served as transporting agents to continuously transport Zn ions across the entire core−shell QDs, germinating the alloying process (Figure 4iv). By repeating this process, the Zn component can be transferred into the CdS shell and then into the CdSe core eventually. This core alloying process (from CdSe to CdZnSe) was in line with the fact that the final positions of first absorption feature (493 nm) and PL peak (509 nm) were located at shorter wavelengths than those of the starting CdSe QDs (absorption at 539 nm, and PL at 550 nm). We did not observe any noticeable Cu impurity emission in the alloy QDs, which was likely due to the minimal amount of Cu addition (~4 Cu per QD),[82,83] and

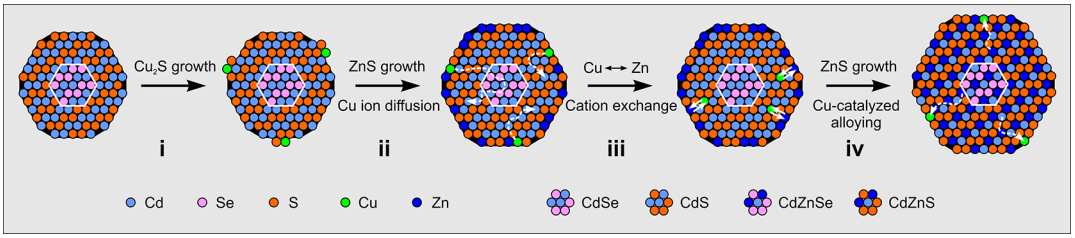

Figure 4. Schematic illustration for Cu-induced alloying process during the synthesis of CdZnSe−CdZnS core−shell alloy QDs.

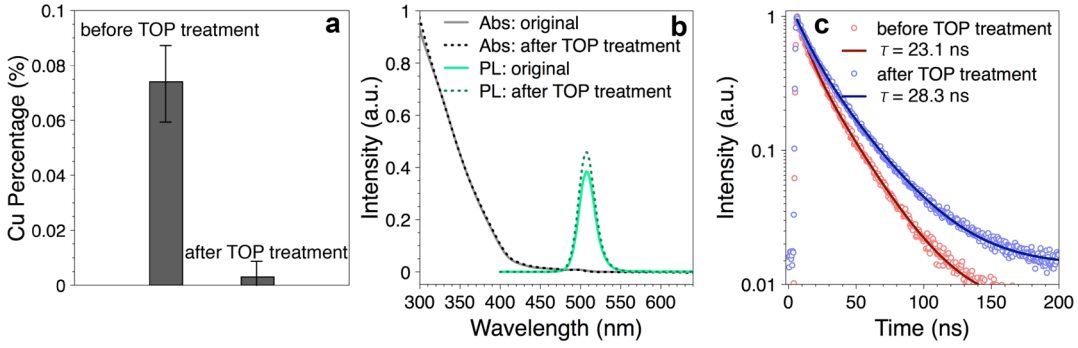

Figure 5. (a) Cu amounts determined by ICP-AES in the as-synthesized alloy QDs before and after TOP treatment. (b) Absorption and PL spectra of the CdZnSe−CdZnS QDs before (solid line) and after (dashed line) TOP treatment. (c) Decay curves of PL lifetimes of the CdZnSe−CdZnS alloy QDs before and after TOP treatment.

DOI: 10.1021/acs.chemmater.9b00557
Chem. Mater. 2019, 31, 2635−2643

commonly observed "self-purification" mechanism in QD systems owing to their finite particle size, thus the increased formation energy of substitutional impurities.[84] Therefore, the Cu ions can "self-purify" and expelled to the surface of QDs during the cooling process after the reaction.[85] Therefore, overall, Cu ions act as catalysts in this alloying process.

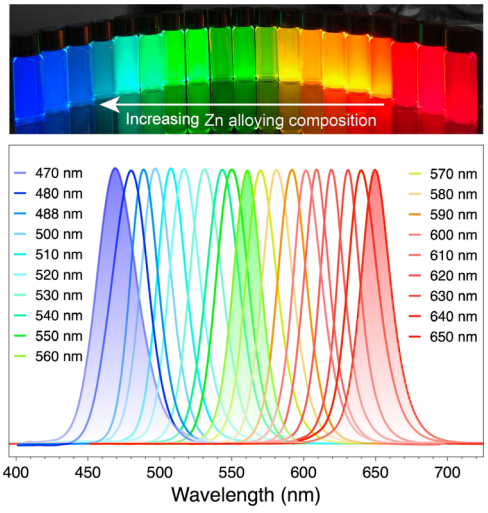

Figure 6. Photograph image (top) and PL spectra (bottom) of the CdSe–CdS core–shell QDs and CdZnSe–CdZnS core–shell alloy QDs showing the full coverage of the visible spectral range from 470 to 650 nm.

To prove the existence of Cu atoms in CdZnSe–CdZnS core–shell alloy QDs, ICP-AES measurement was performed to quantify the Cu amount in the final alloy QDs after purification (see details in the Supporting Information). The ratio between Cu and Cd accessed from ICP-AES was 0.074%, which is approximately equal to the feeding ratio of 0.090%, suggesting the preservation of Cu in the QDs (Figure 5a). As Cu^{+} ions are soft acids (absolute hardness, $\eta = 6.28$ eV) compared to Cd^{2+} ($\eta = 10.29$ eV) and Zn^{2+} ($\eta = 10.88$ eV) cations,[86] it could be expected that Cu would be removed by employing soft bases, such as TOP ($\eta \approx 6$ eV),[87,88] relying on Pearson's HSAB theory.[86,87,89] To examine this speculation, the final CdZnSe–CdZnS QDs were treated with TOP at 250 °C for 5 min (see the Supporting Information).[37] As expected, the amount of Cu in the CdZnSe–CdZnS alloy QDs after the treatment decreased drastically to a nearly background level (Figure 5a and Table S4). This result further supported our hypothesis that Cu ions self-purified and expelled to the surface of the QDs.[84] The absorption spectrum of CdZnSe–CdZnS QDs showed nearly no change after TOP treatment, indicating the intact structural integrity of the QDs (Figure 5b). Although the PL peak position remained the same, its intensity increased by ~7% (the PL QY increased from 57 to 61%), which can be attributed to the reduced trap states by removing Cu impurities (Figure 5b). This removal of defects was further evidenced by the prolongated PL

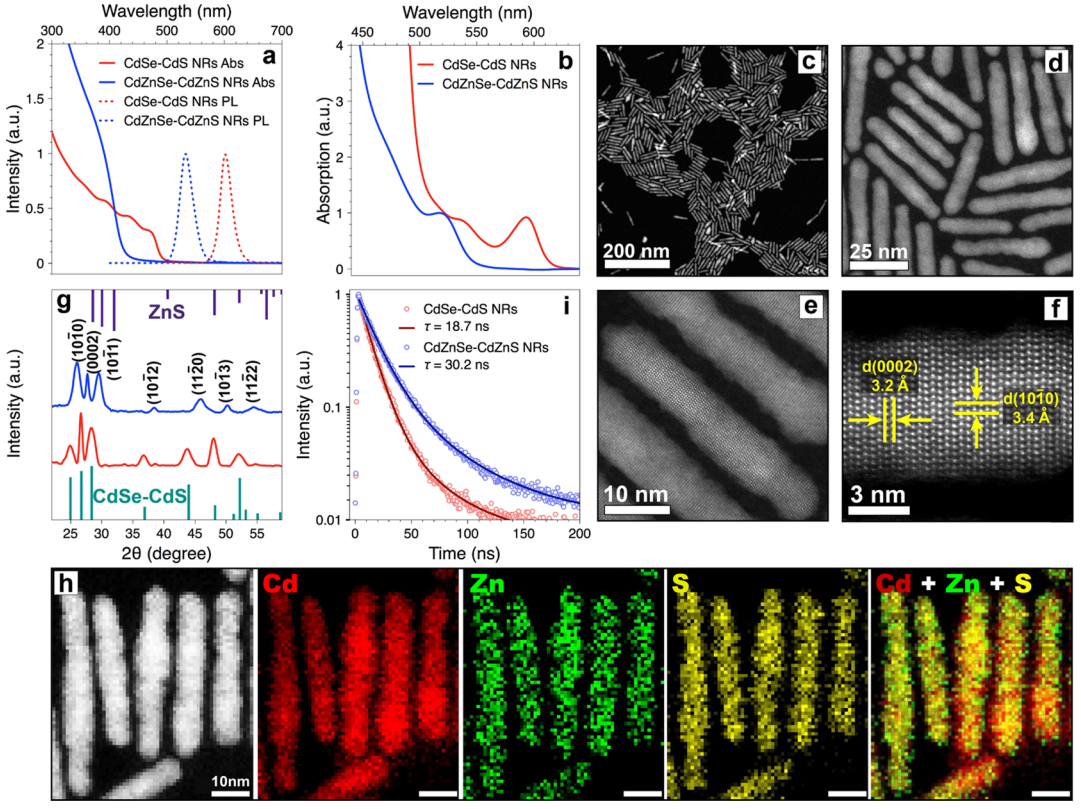

Figure 7. (a) Absorption (solid lines) and PL (dashed lines) spectra of the starting CdSe–CdS NRs (red) and CdZnSe–CdZnS alloy NRs (blue). (b) Zoomed-in spectrum to show the first absorption peak shift comparing the CdSe–CdS NRs to the CdZnSe–CdZnS alloy NRs. (c–f) HAADF-STEM images of the final CdZnSe–CdZnS alloy NRs at different magnifications. (g) XRD spectra of CdSe–CdS NRs and CdZnSe–CdZnS alloy NRs. The green and purple sticks show the positions of XRD peaks for starting CdSe–CdS NRs and bulk WZ-ZnS, respectively. (h) HAADF-STEM image and the corresponding STEM-EELS elemental mappings for Cd, Zn, and S atoms. (i) Decay curves of PL lifetimes of CdSe–CdS NRs and CdZnSe–CdZnS NRs.

DOI: 10.1021/acs.chemmater.9b00557
Chem. Mater. 2019, 31, 2635–2643

lifetime of the QDs (from 23.1 to 28.3 ns) after the TOP treatment (Figures 5c and S7).

We then applied this Cu-catalyzed alloying method to the synthesis of alloy QDs starting from the CdSe−CdS QDs with different CdSe core sizes and CdS shell thicknesses. A wide spectral coverage from 470 to 650 nm (for the center of the PL peaks) with high PL QYs (50−80%) of the obtained CdZnSe−CdZnS core−shell alloy QDs was achieved by tuning the amount of Zn and S precursors (Figures 6 and S8). To further explore the generality of the Cu-induced alloy synthesis, CdSe−CdS core−shell NRs were also examined.[32] A sample of CdSe−CdS NRs with an aspect ratio of 9.4 and emission at 602 nm was successfully converted to CdZnSe−CdZnS alloy NRs with a reduced aspect ratio of 6.2 and a blue-shifted PL peak centered at 534 nm (Figure 7a). Correspondingly, the absorption features of NRs blue-shifted to a shorter wavelength region, accompanied by the decrease of absorption for CdS and increase of absorption for ZnS (Figures 7a,b and S9). TEM and XRD measurements indicated the preservation of shape, uniformity, and WZ crystal structure of the NRs (Figures 7c−g and S10−S13). High-resolution STEM (HR-STEM) images showed cross-fringes of $(10\bar{1}0)$ and (0002) planes with *d*-spacings of 3.4 and 3.2 Å, respectively (Figures 7f and S12). The slightly smaller lattices were obtained by Zn alloying into the CdSe−CdS NRs, which is in good agreement with the XRD data showing red-shifted Bragg diffraction peaks (Figures 7g and S13, Tables S5 and S6). Additionally, the formation of CdZnSe−CdZnS alloy NRs was confirmed indisputably by STEM-electron energy-loss spectroscopy (EELS) elemental mapping results, showing that Zn atoms were fully distributed in the entire NRs (Figures 7h and S14). Time-resolved PL measurements showed that the average PL lifetime increased from 18.7 ns for CdSe−CdS NRs to 30.2 ns for CdZnSe−CdZnS alloy NRs, in line with the increased average volume of single NRs from ∼3900 to ∼6700 nm^3 (Figure 7i). The successful employment of CdSe−CdS NRs suggested that this Cu-induced alloying process is independent of the shape of the starting QDs.

CONCLUSIONS

In conclusion, we demonstrate a new way of fabricating CdZnSe−CdZnS core−shell alloy QDs by using Cu cations as transporting catalysts to effectively transfer a Zn component into CdSe−CdS core−shell QDs. The morphological uniformity, core−shell structure, and crystal phase can be well-preserved from the starting CdSe−CdS QDs during the synthesis. By employing this methodology, high-quality core−shell alloy QDs with high PL QYs and narrow emission profiles covering nearly the full range of the visible spectrum have been synthesized. The mechanistic investigation attributes the alloying process to highly diffusive Cu ions acting as alloying catalysts to transfer the Zn component across the whole CdSe−CdS QDs. Moreover, we show that the remaining surface Cu can be removed with TOP treatment based on the HSAB theory, affording QDs with less surface defects, thus resulting in higher QYs. Finally, we demonstrate that this approach can be easily adapted to the synthesis of CdZnSe−CdZnS NRs, suggesting a generality of this alloying process. Our study sheds light on a new synthetic paradigm of generating various alloy nanocrystals with desired properties through Cu-catalyzed ion diffusion and solid solution alloying processes.

ASSOCIATED CONTENT

Supporting Information

The Supporting Information is available free of charge on the ACS Publications website at DOI: 10.1021/acs.chemmater.9b00557.

Synthetic methods; characterization methods; Cu diffusion rate calculation; absorption and PL spectra, QYs, XRD fittings, TEM and HR-TEM images, HAADF-STEM images, elemental mapping images, EDX data, EPR spectra, ICP data, and lifetime spectra for CdSe−CdS QDs and CdZnSe−CdZnS alloy QDs; absorption and PL spectra and TEM images for control experiment; and absorption and PL spectra, TEM and HR-TEM images, XRD spectra and fittings, HAADF-STEM image, and elemental mapping images for CdZnSe−CdZnS alloy NRs (PDF)

AUTHOR INFORMATION

Corresponding Author

*E-mail: ouchen@brown.edu.

ORCID

Hua Zhu: 0000-0003-2733-7837
Xudong Wang: 0000-0002-1189-8181
Dong Su: 0000-0002-1921-6683
Jing Zhao: 0000-0002-6882-2196
Ou Chen: 0000-0003-0551-090X

Notes

The authors declare no competing financial interest.

ACKNOWLEDGMENTS

O.C. acknowledges the support from Brown University startup funds, the Institute for Molecular and Nanoscale Innovation (IMNI) seed fund, and the National Science Foundation (OIA-1538893). The project described was supported by Institutional Development award number U54GM115677 from the National Institute of General Medical Sciences of the National Institutes of Health, which funds Advance Clinical and Translational Research (Advance-CTR). The content is solely the responsibility of the authors and does not necessarily represent the official views of the National Institutes of Health. TEM measurements were performed at the Electron Microscopy Facility in IMNI at Brown University. J.Z. acknowledges the partial financial support from the National Science Foundation CAREER award (CHE-1554800). This work was supported in part by the award of a Thermo Fisher Scientific Graduate Fellowship to X.W. The TEM studies were partially performed using the facilities in the UConn/Thermo Fisher Scientific Center for Advanced Microscopy and Materials Analysis (CAMMA). Part of electron microscopy work was performed at the Center for Functional Nanomaterials, Brookhaven National Laboratory, which is supported by the U.S. Department of Energy (DOE), Office of Basic Energy Science, under contract DE-SC0012704.

REFERENCES

(1) Chen, O.; Wei, H.; Maurice, A.; Bawendi, M.; Reiss, P. Pure Colors From Core-Shell Quantum Dots. *MRS Bull.* **2013**, *38*, 696−702.
(2) Kovalenko, M. V.; Manna, L.; Cabot, A.; Hens, Z.; Talapin, D. V.; Kagan, C. R.; Klimov, V. I.; Rogach, A. L.; Reiss, P.; Milliron, D. J.; Guyot-Sionnnest, P.; Konstantatos, G.; Parak, W. J.; Hyeon, T.; Korgel,

DOI: 10.1021/acs.chemmater.9b00557
Chem. Mater. 2019, 31, 2635−2643

B. A.; Murray, C. B.; Heiss, W. Prospects of Nanoscience with Nanocrystals. *ACS Nano* **2015**, *9*, 1012−1057.
(3) Nozik, A. J. Quantum Dot Solar Cells. *Phys. E* **2002**, *14*, 115−120.
(4) Kamat, P. V. Quantum Dot Solar Cells. Semiconductor Nanocrystals as Light Harvesters. *J. Phys. Chem. C* **2008**, *112*, 18737−18753.
(5) Lee, H.; Wang, M.; Chen, P.; Gamelin, D. R.; Zakeeruddin, S. M.; Grätzel, M.; Nazeeruddin, M. K. Efficient CdSe Quantum Dot-Sensitized Solar Cells Prepared by an Improved Successive Ionic Layer Adsorption and Reaction Process. *Nano Lett.* **2009**, *9*, 4221−4227.
(6) Lee, Y.-L.; Lo, Y.-S. Highly Efficient Quantum-Dot-Sensitized Solar Cell Based on Co-Sensitization of CdS/CdSe. *Adv. Funct. Mater.* **2009**, *19*, 604−609.
(7) Chuang, C.-H. M.; Brown, P. R.; Bulović, V.; Bawendi, M. G. Improved Performance and Stability in Quantum Dot Solar Cells through Band Alignment Engineering. *Nat. Mater.* **2014**, *13*, 796−801.
(8) Carey, G. H.; Abdelhady, A. L.; Ning, Z.; Thon, S. M.; Bakr, O. M.; Sargent, E. H. Colloidal Quantum Dot Solar Cells. *Chem. Rev.* **2015**, *115*, 12732−12763.
(9) Dahan, M.; Laurence, T.; Pinaud, F.; Chemla, D. S.; Alivisatos, A. P.; Sauer, M.; Weiss, S. Time-Gated Biological Imaging by Use of Colloidal Quantum Dots. *Opt. Lett.* **2001**, *26*, 825−827.
(10) Han, M.; Gao, X.; Su, J. Z.; Nie, S. Quantum-Dot-Tagged Microbeads for Multiplexed Optical Coding of Biomolecules. *Nat. Biotechnol.* **2001**, *19*, 631−635.
(11) Medintz, I. L.; Uyeda, H. T.; Goldman, E. R.; Mattoussi, H. Quantum Dot Bioconjugates for Imaging, Labelling and Sensing. *Nat. Mater.* **2005**, *4*, 435−446.
(12) Franke, D.; Harris, D. K.; Chen, O.; Bruns, O. T.; Carr, J. A.; Wilson, M. W. B.; Bawendi, M. G. Continuous Injection Synthesis of Indium Arsenide Quantum Dots Emissive in the Short-Wavelength Infrared. *Nat. Commun.* **2016**, *7*, 12749.
(13) Panthani, M. G.; Khan, T. A.; Reid, D. K.; Hellebusch, D. J.; Rasch, M. R.; Maynard, J. A.; Korgel, B. A. In Vivo Whole Animal Fluorescence Imaging of a Microparticle-Based Oral Vaccine Containing ($CuInSe_xS_{2-x}$)/ZnS Core/Shell Quantum Dots. *Nano Lett.* **2013**, *13*, 4294−4298.
(14) Colvin, V. L.; Schlamp, M. C.; Alivisatos, A. P. Light-Emitting Diodes Made from Cadmium Selenide Nanocrystals and a Semiconducting Polymer. *Nature* **1994**, *370*, 354−357.
(15) Liu, W.; Howarth, M.; Greytak, A. B.; Zheng, Y.; Nocera, D. G.; Ting, A. Y.; Bawendi, M. G. Compact Biocompatible Quantum Dots Functionalized for Cellular Imaging. *J. Am. Chem. Soc.* **2008**, *130*, 1274−1284.
(16) Pimputkar, S.; Speck, J. S.; DenBaars, S. P.; Nakamura, S. Prospects for LED Lighting. *Nat. Photon.* **2009**, *3*, 180−182.
(17) Jang, E.; Jun, S.; Jang, H.; Lim, J.; Kim, B.; Kim, Y. White-Light-Emitting Diodes with Quantum Dot Color Converters for Display Backlights. *Adv. Mater.* **2010**, *22*, 3076−3080.
(18) Shirasaki, Y.; Supran, G. J.; Bawendi, M. G.; Bulović, V. Emergence of Colloidal Quantum-Dot Light-Emitting Technologies. *Nat. Photon.* **2013**, *7*, 13−23.
(19) Bae, W. K.; Park, Y.-S.; Lim, J.; Lee, D.; Padilha, L. A.; McDaniel, H.; Robel, I.; Lee, C.; Pietryga, J. M.; Klimov, V. I. Controlling the Influence of Auger Recombination on the Performance of Quantum-Dot Light-Emitting Diodes. *Nat. Commun.* **2013**, *4*, 2661.
(20) Mashford, B. S.; Stevenson, M.; Popovic, Z.; Hamilton, C.; Zhou, Z.; Breen, C.; Steckel, J.; Bulovic, V.; Bawendi, M.; Coe-Sullivan, S.; Kazlas, P. T. High-Efficiency Quantum-Dot Light-Emitting Devices with Enhanced Charge Injection. *Nat. Photon.* **2013**, *7*, 407−412.
(21) Yang, Y.; Zheng, Y.; Cao, W.; Titov, A.; Hyvonen, J.; Manders, J. R.; Xue, J.; Holloway, P. H.; Qian, L. High-Efficiency Light-Emitting Devices Based on Quantum Dots with Tailored Nanostructures. *Nat. Photon.* **2015**, *9*, 259−266.
(22) Li, X.; Zhao, Y.-B.; Fan, F.; Levina, L.; Liu, M.; Quintero-Bermudez, R.; Gong, X.; Quan, L. N.; Fan, J.; Yang, Z.; Hoogland, S.; Voznyy, O.; Lu, Z.-H.; Sargent, E. H. Bright Colloidal Quantum Dot Light-Emitting Diodes Enabled by Efficient Chlorination. *Nat. Photon.* **2018**, *12*, 159−164.
(23) Pinaud, F.; Clarke, S.; Sittner, A.; Dahan, M. Probing Cellular Events, One Quantum Dot at a Time. *Nat. Methods* **2010**, *7*, 275−285.
(24) Nagaoka, Y.; Zhu, H.; Eggert, D.; Chen, O. Single-Component Quasicrystalline Nanocrystal Superlattices through Flexible Polygon Tiling Rule. *Science* **2018**, *362*, 1396−1400.
(25) Nagaoka, Y.; Tan, R.; Li, R.; Zhu, H.; Eggert, D.; Wu, Y. A.; Liu, Y.; Wang, Z.; Chen, O. Superstructures Generated from Truncated Tetrahedral Quantum Dots. *Nature* **2018**, *561*, 378−382.
(26) Murray, C. B.; Norris, D. J.; Bawendi, M. G. Synthesis and Characterization of Nearly Monodisperse CdE (E = Sulfur, Selenium, Tellurium) Semiconductor Nanocrystallites. *J. Am. Chem. Soc.* **1993**, *115*, 8706−8715.
(27) Alivisatos, A. P. Semiconductor Clusters, Nanocrystals, and Quantum Dots. *Science* **1996**, *271*, 933−937.
(28) Peng, X.; Manna, L.; Yang, W.; Wickham, J.; Scher, E.; Kadavanich, A.; Alivisatos, A. P. Shape Control of CdSe Nanocrystals. *Nature* **2000**, *404*, 59−61.
(29) Buhro, W. E.; Colvin, V. L. Shape Matters. *Nat. Mater.* **2003**, *2*, 138−139.
(30) Talapin, D. V.; Koeppe, R.; Götzinger, S.; Kornowski, A.; Lupton, J. M.; Rogach, A. L.; Benson, O.; Feldmann, J.; Weller, H. Highly Emissive Colloidal CdSe/CdS Heterostructures of Mixed Dimensionality. *Nano Lett.* **2003**, *3*, 1677−1681.
(31) Talapin, D. V.; Nelson, J. H.; Shevchenko, E. V.; Aloni, S.; Sadtler, B.; Alivisatos, A. P. Seeded Growth of Highly Luminescent CdSe/CdS Nanoheterostructures with Rod and Tetrapod Morphologies. *Nano Lett.* **2007**, *7*, 2951−2959.
(32) Carbone, L.; Nobile, C.; De Giorgi, M.; Sala, F. D.; Morello, G.; Pompa, P.; Hytch, M.; Snoeck, E.; Fiore, A.; Franchini, I. R.; Nadasan, M.; Silvestre, A. F.; Chiodo, L.; Kudera, S.; Cingolani, R.; Krahne, R.; Manna, L. Synthesis and Micrometer-Scale Assembly of Colloidal CdSe/CdS Nanorods Prepared by a Seeded Growth Approach. *Nano Lett.* **2007**, *7*, 2942−2950.
(33) Zhong, H.; Zhou, Y.; Ye, M.; He, Y.; Ye, J.; He, C.; Yang, C.; Li, Y. Controlled Synthesis and Optical Properties of Colloidal Ternary Chalcogenide $CuInS_2$ Nanocrystals. *Chem. Mater.* **2008**, *20*, 6434−6443.
(34) Chen, Y.; Vela, J.; Htoon, H.; Casson, J. L.; Werder, D. J.; Bussian, D. A.; Klimov, V. I.; Hollingsworth, J. A. "Giant" Multishell CdSe Nanocrystal Quantum Dots with Suppressed Blinking. *J. Am. Chem. Soc.* **2008**, *130*, 5026−5027.
(35) Reiss, P.; Protière, M.; Li, L. Core/Shell Semiconductor Nanocrystals. *Small* **2009**, *5*, 154−168.
(36) Cassette, E.; Mahler, B.; Guigner, J.-M.; Patriarche, G.; Dubertret, B.; Pons, T. Colloidal CdSe/CdS Dot-in-Plate Nanocrystals with 2D-Polarized Emission. *ACS Nano* **2012**, *6*, 6741−6750.
(37) Li, H.; Brescia, R.; Krahne, R.; Bertoni, G.; Alcocer, M. J. P.; D'Andrea, C.; Scotognella, F.; Tassone, F.; Zanella, M.; De Giorgi, M.; Manna, L. Blue-UV-Emitting ZnSe(Dot)/ZnS(Rod) Core/Shell Nanocrystals Prepared from CdSe/CdS Nanocrystals by Sequential Cation Exchange. *ACS Nano* **2012**, *6*, 1637−1647.
(38) Morris-Cohen, A. J.; Malicki, M.; Peterson, M. D.; Slavin, J. W. J.; Weiss, E. A. Chemical, Structural, and Quantitative Analysis of the Ligand Shells of Colloidal Quantum Dots. *Chem. Mater.* **2013**, *25*, 1155−1165.
(39) Chen, O.; Zhao, J.; Chauhan, V. P.; Cui, J.; Wong, C.; Harris, D. K.; Wei, H.; Han, H.-S.; Fukumura, D.; Jain, R. K.; Bawendi, M. G. Compact High-Quality CdSe-CdS Core-Shell Nanocrystals with Narrow Emission Linewidths and Suppressed Blinking. *Nat. Mater.* **2013**, *12*, 445−451.
(40) Xie, R.; Zhou, M. Zinc Chalcogenide Seed-Mediated Synthesis of CdSe Nanocrystals: Nails, Chesses and Tetrahedrons. *Chem. Mater.* **2015**, *27*, 3055−3064.
(41) Bladt, E.; van Dijk-Moes, R. J. A.; Peters, J.; Montanarella, F.; de Mello Donega, C.; Vanmaekelbergh, D.; Bals, S. Atomic Structure of Wurtzite CdSe (Core)/CdS (Giant Shell) Nanobullets Related to Epitaxy and Growth. *J. Am. Chem. Soc.* **2016**, *138*, 14288−14293.

DOI: 10.1021/acs.chemmater.9b00557
Chem. Mater. 2019, 31, 2635−2643

(42) Zhou, J.; Pu, C.; Jiao, T.; Hou, X.; Peng, X. A Two-Step Synthetic Strategy toward Monodisperse Colloidal CdSe and CdSe/CdS Core/Shell Nanocrystals. *J. Am. Chem. Soc.* **2016**, *138*, 6475−6483.
(43) Leach, A. D. P.; Macdonald, J. E. Optoelectronic Properties of $CuInS_2$ Nanocrystals and Their Origin. *J. Phys. Chem. Lett.* **2016**, *7*, 572−583.
(44) Tan, R.; Yuan, Y.; Nagaoka, Y.; Eggert, D.; Wang, X.; Thota, S.; Guo, P.; Yang, H.; Zhao, J.; Chen, O. Monodisperse Hexagonal Pyramidal and Bipyramidal Wurtzite CdSe-CdS Core-Shell Nanocrystals. *Chem. Mater.* **2017**, *29*, 4097−4108.
(45) Chen, P. E.; Anderson, N. C.; Norman, Z. M.; Owen, J. S. Tight Binding of Carboxylate, Phosphonate, and Carbamate Anions to Stoichiometric CdSe Nanocrystals. *J. Am. Chem. Soc.* **2017**, *139*, 3227−3236.
(46) Ritchhart, A.; Cossairt, B. M. Templated Growth of InP Nanocrystals with a Polytwistane Structure. *Angew. Chem., Int. Ed. Engl.* **2018**, *57*, 1908−1912.
(47) Dennis, A. M.; Mangum, B. D.; Piryatinski, A.; Park, Y.-S.; Hannah, D. C.; Casson, J. L.; Williams, D. J.; Schaller, R. D.; Htoon, H.; Hollingsworth, J. A. Suppressed Blinking and Auger Recombination in Near-Infrared Type-II InP/CdS Nanocrystal Quantum Dots. *Nano Lett.* **2012**, *12*, 5545−5551.
(48) Tan, R.; Shen, Y.; Roberts, S. K.; Gee, M. Y.; Blom, D. A.; Greytak, A. B. Reducing Competition by Coordinating Solvent Promotes Morphological Control in Alternating Layer Growth of CdSe/CdS Core/Shell Quantum Dots. *Chem. Mater.* **2015**, *27*, 7468−7480.
(49) Liu, Y.-H.; Wang, F.; Hoy, J.; Wayman, V. L.; Steinberg, L. K.; Loomis, R. A.; Buhro, W. E. Bright Core-Shell Semiconductor Quantum Wires. *J. Am. Chem. Soc.* **2012**, *134*, 18797−18803.
(50) Peng, X.; Schlamp, M. C.; Kadavanich, A. V.; Alivisatos, A. P. Epitaxial Growth of Highly Luminescent CdSe/CdS Core/Shell Nanocrystals with Photostability and Electronic Accessibility. *J. Am. Chem. Soc.* **1997**, *119*, 7019−7029.
(51) Dabbousi, B. O.; Rodriguez-Viejo, J.; Mikulec, F. V.; Heine, J. R.; Mattoussi, H.; Ober, R.; Jensen, K. F.; Bawendi, M. G. (CdSe)ZnS Core−Shell Quantum Dots: Synthesis and Characterization of a Size Series of Highly Luminescent Nanocrystallites. *J. Phys. Chem. B* **1997**, *101*, 9463−9475.
(52) Steckel, J. S.; Zimmer, J. P.; Coe-Sullivan, S.; Stott, N. E.; Bulović, V.; Bawendi, M. G. Blue Luminescence from (CdS)ZnS Core-Shell Nanocrystals. *Angew. Chem., Int. Ed. Engl.* **2004**, *43*, 2154−2158.
(53) Li, J. J.; Wang, Y. A.; Guo, W.; Keay, J. C.; Mishima, T. D.; Johnson, M. B.; Peng, X. Large-Scale Synthesis of Nearly Monodisperse CdSe/CdS Core/Shell Nanocrystals Using Air-Stable Reagents via Successive Ion Layer Adsorption and Reaction. *J. Am. Chem. Soc.* **2003**, *125*, 12567−12575.
(54) Hines, M. A.; Guyot-Sionnest, P. Synthesis and Characterization of Strongly Luminescing ZnS-Capped CdSe Nanocrystals. *J. Phys. Chem.* **1996**, *100*, 468−471.
(55) Cao, H.; Ma, J.; Huang, L.; Qin, H.; Meng, R.; Li, Y.; Peng, X. Design and Synthesis of Antiblinking and Antibleaching Quantum Dots in Multiple Colors via Wave Function Confinement. *J. Am. Chem. Soc.* **2016**, *138*, 15727−15735.
(56) Susumu, K.; Field, L. D.; Oh, E.; Hunt, M.; Delehanty, J. B.; Palomo, V.; Dawson, P. E.; Huston, A. L.; Medintz, I. L. Purple-, Blue-, and Green-Emitting Multishell Alloyed Quantum Dots: Synthesis, Characterization, and Application for Ratiometric Extracellular pH Sensing. *Chem. Mater.* **2017**, *29*, 7330−7344.
(57) Zhong, X.; Han, M.; Dong, Z.; White, T. J.; Knoll, W. Composition-tunable $Zn_xCd_{1-x}Se$ nanocrystals with high luminescence and stability. *J. Am. Chem. Soc.* **2003**, *125*, 8589−8594.
(58) Zhong, X.; Feng, Y.; Knoll, W.; Han, M. Alloyed $Zn_xCd_{1-x}S$ Nanocrystals with Highly Narrow Luminescence Spectral Width. *J. Am. Chem. Soc.* **2003**, *125*, 13559−13563.
(59) Kim, S.-W.; Zimmer, J. P.; Ohnishi, S.; Tracy, J. B.; Frangioni, J. V.; Bawendi, M. G. Engineering $InAs_xP_{1-x}$/InP/ZnSe III−V Alloyed Core/Shell Quantum Dots for the Near-Infrared. *J. Am. Chem. Soc.* **2005**, *127*, 10526−10532.
(60) Steckel, J. S.; Snee, P.; Coe-Sullivan, S.; Zimmer, J. P.; Halpert, J. E.; Anikeeva, P.; Kim, L.-A.; Bulovic, V.; Bawendi, M. G. Color-Saturated Green-Emitting QD-LEDs. *Angew. Chem., Int. Ed. Engl.* **2006**, *45*, 5796−5799.
(61) Swafford, L. A.; Weigand, L. A.; Bowers, M. J.; McBride, J. R.; Rapaport, J. L.; Watt, T. L.; Dixit, S. K.; Feldman, L. C.; Rosenthal, S. J. Homogeneously Alloyed CdS_xSe_{1-x} Nanocrystals: Synthesis, Characterization, and Composition/Size-Dependent Band Gap. *J. Am. Chem. Soc.* **2006**, *128*, 12299−12306.
(62) Protière, M.; Reiss, P. Highly Luminescent $Cd_{1-x}Zn_xSe$/ZnS Core/Shell Nanocrystals Emitting in the Blue−Green Spectral Range. *Small* **2007**, *3*, 399−403.
(63) Zhong, X.; Feng, Y.; Zhang, Y.; Gu, Z.; Zou, L. A Facile Route to Violet- to Orange-Emitting Cd_xZn_{1-x} Se Alloy Nanocrystals via Cation Exchange Reaction. *Nanotechnology* **2007**, *18*, 385606.
(64) Bae, W. K.; Nam, M. K.; Char, K.; Lee, S. Gram-Scale One-Pot Synthesis of Highly Luminescent Blue Emitting $Cd_{1-x}Zn_xS$/ZnS Nanocrystals. *Chem. Mater.* **2008**, *20*, 5307−5313.
(65) Groeneveld, E.; Witteman, L.; Lefferts, M.; Ke, X.; Bals, S.; Van Tendeloo, G.; de Mello Donega, C. Tailoring ZnSe-CdSe Colloidal Quantum Dots via Cation Exchange: From Core/Shell to Alloy Nanocrystals. *ACS Nano* **2013**, *7*, 7913−7930.
(66) Lee, K.-H.; Lee, J.-H.; Song, W.-S.; Ko, H.; Lee, C.; Lee, J.-H.; Yang, H. Highly Efficient, Color-Pure, Color-Stable Blue Quantum Dot Light-Emitting Devices. *ACS Nano* **2013**, *7*, 7295−7302.
(67) Shen, H.; Bai, X.; Wang, A.; Wang, H.; Qian, L.; Yang, Y.; Titov, A.; Hyvonen, J.; Zheng, Y.; Li, L. S. High-Efficient Deep-Blue Light-Emitting Diodes by Using High Quality $Zn_xCd_{1-x}S$/ZnS Core/Shell Quantum Dots. *Adv. Funct. Mater.* **2014**, *24*, 2367−2373.
(68) Anikeeva, P. O.; Halpert, J. E.; Bawendi, M. G.; Bulović, V. Quantum Dot Light-Emitting Devices with Electroluminescence Tunable over the Entire Visible Spectrum. *Nano Lett.* **2009**, *9*, 2532−2536.
(69) Cui, J.; Beyler, A. P.; Marshall, L. F.; Chen, O.; Harris, D. K.; Wanger, D. D.; Brokmann, X.; Bawendi, M. G. Direct Probe of Spectral Inhomogeneity Reveals Synthetic Tunability of Single-Nanocrystal Spectral Linewidths. *Nat. Chem.* **2013**, *5*, 602−606.
(70) Cui, J.; Beyler, A. P.; Coropceanu, I.; Cleary, L.; Avila, T. R.; Chen, Y.; Cordero, J. M.; Heathcote, S. L.; Harris, D. K.; Chen, O.; Cao, J.; Bawendi, M. G. Evolution of the Single-Nanocrystal Photoluminescence Linewidth with Size and Shell: Implications for Exciton-Phonon Coupling and the Optimization of Spectral Linewidths. *Nano Lett.* **2016**, *16*, 289−296.
(71) Shim, M.; Guyot-Sionnest, P. Permanent dipole moment and charges in colloidal semiconductor quantum dots. *J. Chem. Phys.* **1999**, *111*, 6955−6964.
(72) Li, L.-s.; Alivisatos, A. P. Origin and Scaling of the Permanent Dipole Moment in CdSe Nanorods. *Phys. Rev. Lett.* **2003**, *90*, 097402.
(73) Peng, Z. A.; Peng, X. Mechanisms of the Shape Evolution of CdSe Nanocrystals. *J. Am. Chem. Soc.* **2001**, *123*, 1389−1395.
(74) Jain, P. K.; Amirav, L.; Aloni, S.; Alivisatos, A. P. Nanoheterostructure Cation Exchange: Anionic Framework Conservation. *J. Am. Chem. Soc.* **2010**, *132*, 9997−9999.
(75) Denton, A. R.; Ashcroft, N. W. Vegard's Law. *Phys. Rev. A* **1991**, *43*, 3161−3164.
(76) Hyun, K.; Lee, J. H.; Yoon, C. W.; Kwon, Y. The Effect of Platinum Based Bimetallic Electrocatalysts on Oxygen Reduction Reaction of Proton Exchange Membrane Fuel Cells. *Int. J. Electrochem. Sci.* **2013**, *8*, 11752−11767.
(77) Sullivan, G. A. Diffusion and Solubility of Cu in CdS Single Crystals. *Phys. Rev.* **1969**, *184*, 796−805.
(78) Knowles, K. E.; Hartstein, K. H.; Kilburn, T. B.; Marchioro, A.; Nelson, H. D.; Whitham, P. J.; Gamelin, D. R. Luminescent Colloidal Semiconductor Nanocrystals Containing Copper: Synthesis, Photophysics, and Applications. *Chem. Rev.* **2016**, *116*, 10820−10851.
(79) Srivastava, B. B.; Jana, S.; Pradhan, N. Doping Cu in Semiconductor Nanocrystals: Some Old and Some New Physical Insights. *J. Am. Chem. Soc.* **2011**, *133*, 1007−1015.

DOI: 10.1021/acs.chemmater.9b00557
Chem. Mater. 2019, 31, 2635−2643

(80) Whitham, P. J.; Knowles, K. E.; Reid, P. J.; Gamelin, D. R. Photoluminescence Blinking and Reversible Electron Trapping in Copper-Doped CdSe Nanocrystals. *Nano Lett.* **2015**, *15*, 4045−4051.
(81) Shannon, R. D. Revised Effective Ionic Radii and Systematic Studies of Interatomic Distances in Halides and Chalcogenides. *Acta Crystallogr.* **1976**, *32*, 751−767.
(82) Jawaid, A. M.; Chattopadhyay, S.; Wink, D. J.; Page, L. E.; Snee, P. T. Cluster-Seeded Synthesis of Doped CdSe:Cu4 Quantum Dots. *ACS Nano* **2013**, *7*, 3190−3197.
(83) Yang, L.; Knowles, K. E.; Gopalan, A.; Hughes, K. E.; James, M. C.; Gamelin, D. R. One-Pot Synthesis of Monodisperse Colloidal Copper-Doped CdSe Nanocrystals Mediated by Ligand-Copper Interactions. *Chem. Mater.* **2016**, *28*, 7375−7384.
(84) Dalpian, G. M.; Chelikowsky, J. R. Self-Purification in Semiconductor Nanocrystals. *Phys. Rev. Lett.* **2006**, *96*, 226802.
(85) Erwin, S. C.; Zu, L.; Haftel, M. I.; Efros, A. L.; Kennedy, T. A.; Norris, D. J. Doping Semiconductor Nanocrystals. *Nature* **2005**, *436*, 91.
(86) Pearson, R. G. Absolute Electronegativity and Hardness: Application to Inorganic Chemistry. *Inorg. Chem.* **1988**, *27*, 734−740.
(87) Pearson, R. G. Chemical Hardness and Bond Dissociation Energies. *J. Am. Chem. Soc.* **1988**, *110*, 7684−7690.
(88) Jain, P. K.; Beberwyck, B. J.; Fong, L.-K.; Polking, M. J.; Alivisatos, A. P. Highly Luminescent Nanocrystals From Removal of Impurity Atoms Residual From Ion-Exchange Synthesis. *Angew. Chem., Int. Ed. Engl.* **2012**, *51*, 2387−2390.
(89) Parr, R. G.; Pearson, R. G. Absolute Hardness: Companion Parameter to Absolute Electronegativity. *J. Am. Chem. Soc.* **1983**, *105*, 7512−7516.

DOI: 10.1021/acs.chemmater.9b00557
Chem. Mater. 2019, 31, 2635−2643